A Bispecific METxMET Antibody–Drug Conjugate with Cleavable Linker Is Processed in Recycling and Late Endosomes

Andres E. Perez Bay[1], Devon Faulkner[1], John O. DaSilva[1], Tara M. Young[1], Katie Yang[1], Jason T. Giurleo[2], Dangshe Ma[2], Frank J. Delfino[2], William C. Olson[2], Gavin Thurston[1], Christopher Daly[1], and Julian Andreev[1]

ABSTRACT

Most antibody–drug conjugates (ADC) approved for the treatment of cancer contain protease-cleavable linkers. ADCs that traffic to lysosomes traverse highly acidic late endosomes, while ADCs that recycle to the plasma membrane traffic through mildly acidic sorting and recycling endosomes. Although endosomes have been proposed to process cleavable ADCs, the precise identity of the relevant compartments and their relative contributions to ADC processing remain undefined. Here we show that a METxMET biparatopic antibody internalizes into sorting endosomes, rapidly traffics to recycling endosomes, and slowly reaches late endosomes. In agreement with the current model of ADC trafficking, late endosomes are the primary processing site of MET, EGFR, and prolactin receptor ADCs. Interestingly, recycling endosomes contribute up to 35% processing of the MET and EGFR ADCs in different cancer cells, mediated by cathepsin-L, which localizes to this compartment. Taken together, our findings provide insight into the relationship between transendosomal trafficking and ADC processing and suggest that receptors that traffic through recycling endosomes might be suitable targets for cleavable ADCs.

Introduction

Antibody–drug conjugates (ADC) specifically bind to a tumor-specific antigen, internalize into the cell and release a cytotoxic payload (1–3). Most ADCs approved for the treatment of cancer contain hydrolysable or enzyme-cleavable linkers bridging the antibody (Ab) and payload (cleavable ADCs), the only two exceptions being ADCs targeting HER2 (trastuzumab-emtansine) and BCMA (belantamab mafodotin; refs. 4, 5). Cleavable valine-citrulline (VC) linkers were designed to be processed in the lysosomes by Cathepsin B, a cysteine protease overexpressed in tumor cells (6). It was later shown that a fraction of VC linker processing happens rapidly after internalization and before the ADC reaches the lysosomes (7). In addition, other cysteine proteases such as Cathepsin S, K, and L (CTSL1) can process VC linkers in the absence of Cathepsin B (8). Therefore, it was proposed that cleavable ADCs that recycle to the plasma membrane can release their payload in the lumen of endosomes (2, 9).

Rapidly recycling receptors, such as the transferrin and EGF receptors (TFRC, EGFR) are internalized into Rab5-positive sorting endosomes (pH 6) and then recycle to the plasma membrane either directly within 2 minutes or through a 15-minute pathway that traverses Rab11-positive recycling endosomes (pH 6.5; ref. 10). In contrast, fast-turnover receptors like PRLR (11) traffic from sorting endosomes to Rab7-positive late endosomes (pH 5.5) that contain abundant proteases enroute to the lysosomes (12). Transendosomal trafficking is tightly regulated by a complex molecular machinery including Rab small GTPases, clathrin and its adaptors, cytoskeleton, molecular motors, snare proteins, and various molecular complexes such as the retromer, ESCORT, and others (13–19).

An important unresolved issue in the ADC field is whether cleavable ADCs can be significantly processed in the mildly acidic environment of early sorting and recycling endosomes or whether efficient processing requires trafficking to late endosomes and lysosomes. Substantial processing in early endosomes would allow the use of recycling receptors as targets of cleavable ADCs, which are currently underutilized. To address this question, we examined a clinical-stage METxMET biparatopic Ab (NCT04077099) and its corresponding ADC (NCT04982224), which is conjugated to a maytansinoid payload via a protease-cleavable VC linker (METxMET-VC-ADC; ref. 20). We had previously shown that METxMET bispecific Ab partially redirects internalized MET from the recycling pathway toward the degradative pathway and therefore traffics through all major endosomal compartments of the cell, which makes it an ideal prototype to study transendosomal trafficking (21).

Here we show that a METxMET biparatopic antibody internalizes into sorting endosomes, rapidly traffics to recycling endosomes (Rab11a-dependent) and slowly reaches late endosomes (Rab5c-dependent). In agreement with the current model of ADC trafficking, late endosomes are the primary processing site of a VC linker biosensor conjugated to MET, EGFR, and PRLR ADCs. Interestingly, recycling endosomes contribute up to 35% VC linker processing of the MET and EGFR ADCs partly mediated by cathepsin-L, which localizes to this compartment. Delaying exit from sorting endosomes toward recycling and late endosomes inhibits ADC processing and cytotoxicity, underscoring the importance of transendosomal trafficking for ADC efficacy. Our work uncovers recycling endosomes as a major site for cleavable ADC processing and suggest that receptors that traffic through this compartment might be suitable targets for cleavable ADCs.

[1]Oncology and Angiogenesis Department, Regeneron Pharmaceuticals, Inc., Tarrytown, New York, New York. [2]Therapeutic Proteins Department, Regeneron Pharmaceuticals, Inc., New York, New York.

Corresponding Author: Andres E. Perez Bay, Regeneron Pharmaceuticals, 777 Old Saw Mill River Road, Tarrytown, NY 10591-6707. Phone: 914-847-3785; E-mail: andres.perezbay@regeneron.com

Mol Cancer Ther 2023;22:357–70

doi: 10.1158/1535-7163.MCT-22-0414

Materials and Methods

Antibodies and other reagents

Fully human antibodies were generated in VelocImmune mice using methods described previously (22, 23). The biparatopic METxMET antibody (Patent US2018/ 0134794A Example 5) was generated using methods described previously (24). To generate METxMET-M114 or -M1 (Patent US2018/0134794A Examples 21 and 22), METxMET antibody in 50 mmol/L HEPES, 150 mmol/L NaCl, pH 8.0, and 10%–15% (v/v) DMA was conjugated with a 5- to 6-fold excess of SMCC-DM1 diaste- reomer or maytansin-3-N-methyl-L-alanine-N-Mebeta-alanine-car- bamyl-(p-amino)benzyl-citrulline-valineadipoyl-succinate (M114). Excess payload was removed by molecular adsorption using activated charcoal. The conjugates were buffer exchanged into formulation buffer (PBS plus 5% glycerol), purified by size-exclusion chromatography or ultrafiltration and sterile filtered. Protein concentrations were determined by UV spectral analysis. Size-exclusion high performance liquid chromatography (HPLC) established that all conjugates used were >90% monomeric, and RP-HPLC established that there was <1% unconjugated linker payload. All conjugated antibodies were analyzed by UV for linker-payload loading values according to (25) and/or by mass difference, native versus conjugated. The METxMET antibody and METxMET-VC-ADC were validated using methods described previously (20, 21). The PRLR Ab (Patent US2022/0008548) and EGFR Ab ("in-house cetuximab" human monoclonal antibody with primary sequence identical to that of cetuximab. Patent US6217866B1) were generated using methods described previously (11).

Commercial Ab was obtained from the following sources: Rab11a (Invitrogen), HER2 (Dako), EGFR (Cell Signaling Technology), Actin-HRP (Santa Cruz Biotechnology), Rab5a, Rab5c, Rab7a, Lamp1 (Abcam), cathepsin-L (RnD and Invitrogen). Fluorescently labeled human FAb and horseradish peroxidase–conjugated FAb were form Jackson ImmunoResearch Laboratories. The METxMET-AF647 was labeled using NHS-modified AF647 fluorophore (Thermo Fisher Scientific) in Dulbecco's phosphate-buffered saline (DPBS) pH8 following manufacturer instructions. Cycloheximide, monensin, brefeldin A, simvastatin, LY294002, bortezomib, lactasistin, nocodazole, CK666, CK869, phalloidin, narciclasine, bafilomycin A, chloroquine, and chaetoglobosin A were purchased from Sigma-Aldrich. Dynasore was purchased from Abcam.

Cell lines

Wild-type human EBC1 (EBC1/WT), NCI-H441, NCI-H1993, SNU-5, T47D, and HeLa cells were obtained from the ATCC, cultured in the manufacturer's recommended media up to passage 15–20, authenticated by short tandem repeat profiling and *Mycoplasma* tested in the last 1–3 years (IDEXX BioResearch).

EBC1/WT cells were engineered to stably express Cas9 nuclease by lentiviral infection (pLentiCas9-Blast) and selection with blasticidin (EBC1/Cas9). To generate EBC1/Cas9 cells stably knocked out for Rab11a and Rab5c, cells were plated in tissue culture-treated 12-well plates (Corning) at 200,000 cells/well. On day 2, cells were preincubated with 5 μg/mL polybrene for 30 minutes at 37°C and infected with lentiviruses (pLenti-H1-gRNA, Gentarget) for 24 hours at a multiplicity of infection of 4. Puromycin selection was initiated 2 days after infection. The lentiviruses encoded guide RNA against Rab11a (GCACAGATATGGGACACAGC, GAGTGATCTACGTCATCTCA or CATGTCTCCAAGCAACAATG), Rab5c (CAAGATCTGTCAATTTAAGC, TCCTCAGGATACATTTGCAC, TCCAGGCCGAAACCGAGGTG) or control (GTCTCCACGCGCAGTACATT). Knockout efficiency was determined by Western blot (WB) analysis and cells were used for experiments up to six passages after the beginning of selection or until an increase in the target expression was observed.

To generate EBC1 cells expressing endosomal markers, EBC1/WT cells were infected with the same protocol as above. The lentiviruses (Gentarget) encoded cDNA sequences of Rab5c (GenBank: U18420.1), Rab11a (GenBank: AF000231.1), or Rab7a (GenBank: AF050175.1), terminally fused to the N-terminus of GFP under the control of suCMV promoter. Puromycin selection was initiated 2 days after infection and cells were sorted for GFP-positive expression. To transciently knock down cathepsin-L in EBC1/WT, EBC1/Rab11a-GFP or EBC1/Rab5c-GFP, 10,000 cells were plated in collagen-coated, 96-well optical plates (Greiner #655956). Transfections were performed the next day with 5 pmol siRNA (Dharmacon #J-005841-11-0005; Invitrogen #4390824) and 0.25 μL Lipofectamine RNAiMax (Invitrogen) in a final volume of 100 μL Optimem (Invitrogen) per well. METxMET-VC-biosensor assays were performed 3 days post-transfection as described below and samples were lysed to determine cathepsin-L knockdown efficiency with WB analysis.

CRISPR screen

EBC1/Cas9 cells were plated in collagen-coated, 96-well optical plates (Greiner #655956) at 20,000 cells/well. A total of 24 hours later, cells were transiently transfected in triplicate with synthetic guide and tracer RNAs (Dharmacon), from 20 μmol/L stocks re-supended in 10 mmol/L TRIS RNAse-free water. The 6-hour transfection was performed in 100 μL/well Optimem containing 0.5 μL Dharmafect 4, 100 nmol/L guide RNA, and 100 nmol/L tracer RNA.

A total of 72 hours after transfection, an internalization assay was performed. Briefly, METxMET-AF647 (10 μg/mL) was bound to the cell surface of the cells for 20 minutes at 4°C. After washing the unbound Ab, cells were allowed to internalize for 60 minutes at 37°C and the fraction METxMET-AF647 that remained in the cell surface after the internalization period was stained with anti-human-AF488 Fab (4 μg/mL) for 20 minutes at 4°C. After washing the unbound Fab, cells were fixed with 4% paraformaldehyde 0.075% Saponin and 1 μg/mL Hoechst for 10 minutes at room temperature and washed with 100 μL DPBS before acquisition.

Acquisition was performed with an Image Express epifluorescence high content system (Molecular Devices) using a 40X objective and filter cubes optimized for AF405, AF488, and AF647 fluorophores. A total of 25 fields/well were acquired with a 650 μm distance between each other ensuring a homogenous coverage of peripheral and central areas of the well. Integrated fluorescence of the three fluorophores was subtracted from local background. The signal of the AF488-Fab (surface METxMET Ab) was further used to determine the effect of gene knockout on METxMET Ab trafficking.

Spinning disc confocal system

Confocal images were acquired with a Zeiss spinning disk inverted system using a 40x, 1.47NA oil immersion objective, EMCCD evolve camera, excitation lasers of 405, 488, 561, and 647 nm and band pass emission filters of 450/50, 525/50, 629/62, and 690/50 nm. An environment-controlled chamber was set to 37°C and 5% CO_2 for live cell imaging.

Internalization assay

The internalization kinetics of METxMET Ab was assessed in fixed cells using methods described previously (26). Genetically engineered or dynasore-treated EBC1 cells were incubated with METxMET-AF647 (10 μg/mL) for 20 minutes at 4°C. Unbound

antibody was washed off and endocytosis was initiated by transferring the cells to 37°C for various times. At each timepoint, METxMET Ab remaining on the cell surface was detected with AF488-conjugated goat anti-human Fab fragment (4 μg/mL) for 20 minutes at 4°C. Afterward, cells were fixed with 4% paraformaldehyde, 0.075% Saponin, and 1 μg/mL Hoechst for 10 minutes at room temperature. Surface METxMET was quantified by the colocalization of METxMET-AF647 with anti-human-AF488 Fab using the Manders' colocalization coefficient (MCC) and normalized to t_0 in a pixel by pixel basis in nine confocal fields/condition.

Recycling assay

The recycling kinetics of METxMET Ab were assessed with confocal live imaging using methods described previously (26). EBC1/Cas9 control and knockout cells were incubated with METxMET-AF647 (10 μg/mL) for 20 minutes at 4°C. Unbound antibody was washed off and cells were then transferred to 37°C for 60 minutes to allow antibody internalization. Any METxMET-AF647 remaining on the cell surface at the end of this period was blocked with unlabeled anti-human Fab (4 μg/mL) for 20 minutes at 4°C. To label recycling METxMET-AF647, cells were incubated with AF488-labeled anti-human Fab (2 μg/mL) for 10 minutes at 4°C and transferred to the environment-controlled chamber for live imaging acquisition. The mean fluorescence intensity (MFI) of AF647 and AF488 was measured on a pixel-by-pixel basis in nine confocal fields/well. METxMET Ab recycling was determined as AF488 signal over time normalized to the amount of METxMET-AF647 at the beginning of the experiment (i.e., AF488 $MFI_{(ti)}$/AF647 $MFI_{(t0)}$) and expressed as percentage of the maximum recycling observed in the control condition.

METxMET-VC-biosensor processing assay

The biosensors were conjugated to METxMET Ab using NHS chemistry, as reported previously (27). The processing kinetics of METxMET-biosensor Ab were assessed with confocal live imaging as follows. EBC1/Cas9 control and knockout cells were incubated with METxMET-VC-bisensor (10 μg/mL) for 20 minutes at 4°C. Unbound antibody was washed off and endocytosis was initiated by transferring the cells to the environment-controlled chamber for live imaging acquisition. The amount of biosensor cleavage was directly proportional to the AF568 signal. The MFI of AF647 (total METxMET) and AF568 (cleaved biosensor) was measured on a pixel-by-pixel basis in nine confocal fields/well. METxMET Ab processing was determined as the AF568 signal over time normalized to the amount of METxMET-AF647 at the beginning of the experiment (i.e., AF568 $MFI_{(t)}$/AF647 $MFI_{(t0)}$) and expressed as percentage of the maximum processing observed in the control condition.

METxMET-VC-biosensor internalization and processing triple colocalization assay

A triple colocalization assay was developed to simultaneously determine three fractions of METxMET-VC-biosensor in fixed EBC1/Cas9 cells after 60 minutes internalization: surface/intact, internalized/intact, and internalized/processed. The percentage of total METxMET-VC-biosensor present at the cell surface was quantified as the percentage colocalization of AF647 (total) with AF488 (surface) on a pixel-by-pixel basis, using MCC in nine confocal fields/well. The percentage of total METxMET-VC-bisensor processed was quantified as the percentage colocalization of AF647 (total) with AF568 (processed) on a pixel-by-pixel basis, using MCC in nine confocal fields/well. The percentage of total METxMET-VC-bisensor that was internalized but not processed (intact) was estimated by the formula: 100% − (% surface + % processed). For this assay, cells were treated with the following inhibitors: 25 μmol/L monensin, 7 μmol/L brefeldin A, 25 μmol/L simvastatin, 25 μmol/L LY294002, 25um bortezomib, 25 μmol/L lactacistin, 17 μmol/L nocodazole, 25 μmol/L CK666, 25 μmol/L CK869, 25 μmol/L phalloidin, 25 μmol/L narciclasine, 3 μmol/L bafilomycin A, 25 μmol/L chloroquine, 25 μmol/L chaetoglobosin A, 50 μmol/L dynasore.

Transendosomal trafficking assay

The trafficking and processing kinetics of METxMET Ab in different endosomes was assessed with confocal live imaging using methods described previously (28, 29). EBC1/WT cells stably expressing Rab5c-GFP, Rab11a-GFP, or Rab7a-GFP were incubated with METxMET-biosensor (10 μg/mL) for 20 minutes at 4°C. Unbound antibody was washed off and endocytosis was initiated by transferring the cells to the environment-controlled chamber for live imaging acquisition. The colocalization of METxMET-AF647 with Rab5c-GFP, Rab11a-GFP or Rab7a-GFP, respectively was quantified over time using MCC in a pixel by pixel basis in four to five regions of interest (ROI) containing one to five cells each (i.e., colocalization Pixels/AF647 $pixels)_{ti}$. Processing at sorting, recycling or late endosomes was quantified by determining the integrated fluorescence of the processed METxMET-VC-biosensor (AF568) and calculating the percentage of this signal that colocalizes with either Rab5-GFP, Rab11-GFP, or Rab7-GFP using the above method. Analysis was performed in a pixel by pixel basis in four to five ROIs containing one to five cells each

Immunofluorescence

EBC1/Cas9 cells incubated with METxMET-AF647 (10 μg/mL) for the indicated times were washed with cold medium, fixed with 4% paraformaldehyde DPBS for 10 minutes, permeabilized with 0.1% triton DPBS for 10 minutes and blocked in 1% BSA DPBS for 60 minutes at room temperature. Primary antibodies were incubated in 1% BSA DPBS overnight at 4°C and secondary FAb were incubated in 1% BSA DPBS for 60 minutes at room temperature. Cells were washed three times after each incubation with 1% BSA DPBS for 5 minutes at room temperature.

Protein turnover assay and WB analysis

EBC1/Cas9 control and knockout cells were incubated with 50 μg/mL cycloheximide at 37°C. At the indicated times, cells were lysed in RIPA buffer and processed for WB analysis. Cell lysates were resolved on 4% to 20% Tris-Glycine gels (Invitrogen) and blotted to polyvinylidene difluoride membranes (Bio-Rad) using a Trans-blot turbo transfer system (Bio-Rad). Membranes were blocked with 1% milk in TBS for 1–2 hours at room temperature. Primary antibodies were incubated overnight at 4°C and secondary peroxidase–conjugated secondary antibodies were incubated for 1 hour at room temperature. Chemiluminescence signal was detected with West pico plus substrate (Thermo Fisher Scientific).

Apoptosis assay

EBC1 cells were plated in collagen-coated, 96-well optical plates (Greiner #655956) at 15,000 cells/well. A total of 24 hours after plating, cells were treated with control or METxMET Ab directly conjugated to a maytansinoid derivative payload through a protease-cleavable VC linker. A total of 100 μmol/L dynasore, 3 μmol/L bafilomycin A, 1.6 μmol/L chaetoglobosin A, or control DMSO were added simultaneously with the ADCs. A total of 2 μmol/L caspase3/7

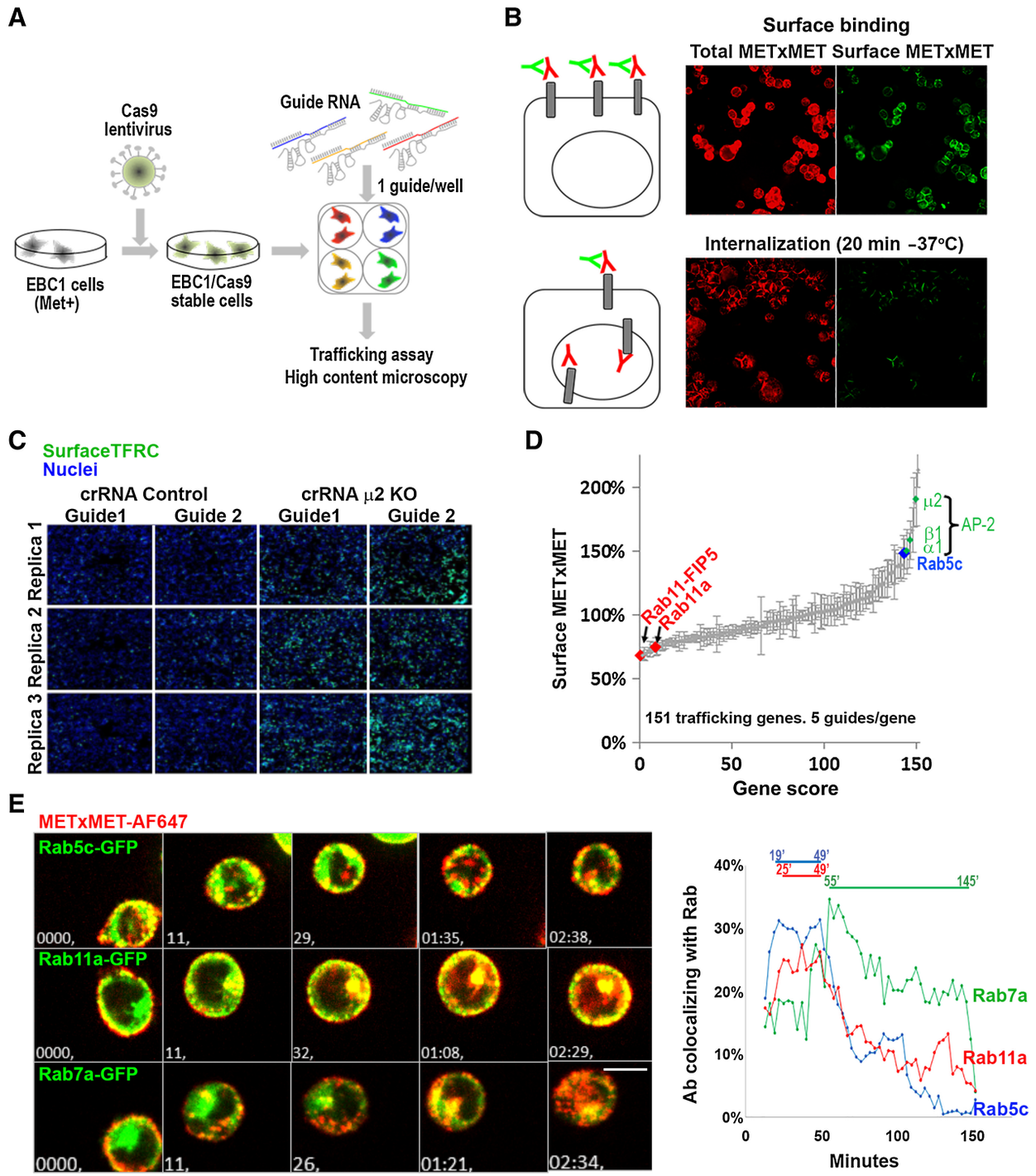

Figure 1.

An arrayed CRISPR screen uncovers opposing effects of Rab5c and Rab11a on METxMET Ab trafficking. **A,** EBC1 cells stably expressing Cas9 were transiently transfected with guide RNAs targeting 151 genes involved in protein trafficking (5 guides/gene). Three days after transfection, internalization of METxMET Ab conjugated with Alexa Fluor 647 (METxMET-AF647) was determined with high-content microscopy. **B,** METxMET-AF647 was prebound to the surface of EBC1 cells on ice (total METxMET) and then allowed to internalize for 0 or 20 minutes at 37°C. Noninternalized Ab was stained with anti-human-AF488 Fab (surface METxMET). Loss of AF488 signal reflects the disappearance of the METxMET-AF647 from the cell surface after the net effect of endocytosis and recycling. Single field images shown. **C,** High-content microscopy and the trafficking assay explained above show that silencing of the mu2 subunit of the clathrin adaptor AP-2 increases surface TFRC. Multiple field images shown. **D,** Arrayed CRISPR screen reveals that silencing of Rab5c or Rab11a (and its downstream effector Rab11-FIP5) have opposite effects on surface METxMET-AF647. **E,** Internalization time course of prebound METxMET-AF647 recorded with confocal live imaging in EBC1 cells stably expressing either Rab5c-GFP, Rab11a-GFP, or Rab7a-GFP. Trafficking to sorting, recycling, or late endosomes was quantified by the colocalization of METxMET-AF647 (red) with Rab5c-GFP, Rab11a-GFP, or Rab7a-GFP, respectively (green), using MCC. Representative images (left) and quantification (right) from four to five ROIs containing one to five cells each. Scale bar: 10 μm.

dye (Incucyte) was also added with the treatment to detect apoptotic cells. A total of 24 hours after treatment, cells were fixed with 4% paraformaldehyde, 0.075% Saponin, and 1 μg/mL Hoechst for 10 minutes at room temperature and washed with 100 μL DPBS before acquisition. Acquisition was performed with an Image Express epifluorescence high content system (Molecular Devices) using a 20X objective and filter cubes optimized for AF405 and AF488 fluorophores. Nine fields/well were acquired covering approximately 80% of the well area. The number of total and apoptotic cells was quantified by applying a segmentation algorithm to the Hoechst (total) and caspase 3/7 dye (apoptotic) signals. The percentage of apoptotic cells was expressed as the ratio of caspase3/7 dye-positive cells over Hoechst-positive nuclei.

Xenograft studies

All mouse experiments were conducted in accordance with the guidelines of and approved by the Regeneron Institutional Animal Care and Use Committee. Six-week-old female SCID mice (Jackson LAb, 001803) were injected with 150 μL EBC1 cell suspension in matrigel (Corning) at 33 million cells per milliliter. A total of 10 days after implantation tumors measuring approximately 200 mm^3 were injected with 5 μg/mL METxMET Ab or METxMET-VC-biosensor. A total of 24 hours after injection, tumors were harvested, fixed with 30% sucrose-DPBS (3 hours, 4°C) followed by 4% PFA-DPBS (16 hours, 4°C) with gentle rotation. Fixed tumors were embedded in optimal cutting temperature compound (Tissue-Tek), flash frozen, cut in think sections and processed for immunofluorescence staining and confocal imaging.

Tissue sections were permeabilized with 0.1% Triton X-100 (Sigma)-DPBS (10 minutes, room temperature), blocked with 1% BSA-DPBS (60 minutes, room temperature) and incubated with primary antibodies previously labeled with Alexa fluorophores (Thermo Fisher Scientific) in 1% BSA-DPBS (60 minutes, room temperature). Samples were washed twice with 1% BSA-DPBS, once with DPBS (5 minutes, room temperature), covered with mounting medium (biotium) and sealed before imaging.

Data availability statement

Data sharing is not applicable to this article as no data were created or analyzed in this study.

Results

A CRISPR knockout trafficking screen reveals that Rab11a and Rab5c have divergent effects on METxMET Ab trafficking

A CRISPR knockout screen was performed to elucidate the transendosomal pathways and molecular machinery underlying METxMET antibody trafficking. EBC1 lung cancer cells stably expressing Cas9 nuclease were transiently transfected with a library of synthetic CRISPR RNAs targeting 151 genes involved in endocytosis, recycling, degradation, and transendosomal trafficking (**Fig. 1A**; Supplementary Table S1). On posttransfection day 3, Alexa647-labeled METxMET antibody (METxMET Ab) was prebound to EBC1 cell surface and allowed to internalize for 60 minutes. Noninternalized METxMET Ab was stained with anti-human-AF488 Fab and quantified with high-content microscopy. METxMET Ab internalization caused a substantial loss of anti-human-AF488 Fab signal (**Fig. 1B**). A positive control showed that CRISPR-mediated deletion of the mu2 subunit of the clathrin adaptor AP-2 strongly increased surface levels of TFRC (**Fig. 1C**). The screen results showed that deletion of three of the four subunits of AP-2 (mu2, alpha1, and beta1) significantly increased surface METxMET Ab (**Fig. 1D**), suggesting clathrin-mediated internalization (30) and underscoring the ability of the screen to identify different genes within the same molecular pathway. Moreover, deletion of the small GTPase Rab5c increased METxMET Ab surface levels, while deletion of Rab11a and its downstream effector Rab11-FIP5 had the opposite effect. This is consistent with the reported roles of Rab5c in sorting-to-late endosome maturation and of Rab11a on receptor recycling to the plasma membrane (31–34).

METxMET Ab traffics through sorting, recycling, and late endosomes in EBC1 cells

The CRISPR screen suggests that METxMET Ab traffics through Rab5c-positive sorting endosomes and Rab11a-positive recycling endosomes but does not inform on the sequence of arrival, trafficking kinetics, and residence times in each endosomal compartment. The endosomal itinerary of METxMET Ab was studied with confocal live imaging in EBC1 cells stably expressing markers of sorting (Rab5c-GFP), recycling (Rab11a-GFP), or late (Rab7a-GFP) endosomes (33, 35–37; Supplementary Fig. S1a). METxMET Ab rapidly reached sorting endosomes (peak colocalization with Rab5c-GFP at 19 minutes, 30-minute residence time; **Fig. 1E**). Interestingly, successive colocalization peaks of gradually diminishing amplitude were observed every 48 minutes, suggesting that METxMET Ab undergoes multiple rounds of recycling between endosomes and the plasma membrane (Supplementary Fig. S1b). Only 6 minutes after reaching sorting endosomes, METxMET Ab arrived in recycling endosomes (peak colocalization with Rab11a-GFP at 25 minutes, 24-minute residence time). In contrast, arrival to late endosomes occurred after a 25-minute delay (peak colocalization with Rab7a-GFP at 55 minutes, 90-minute residence time), which coincided with a large efflux from sorting endosomes (**Fig. 1E**). Internalized METxMET Ab showed qualitatively similar kinetics in fixed EBC1 cells immunostained for endogenous Rab5c, Rab11a, and Rab7a, suggesting that Rab-GFPs overexpression does not cause major changes in METxMET Ab trafficking (Supplementary Fig. S2). This experiment also underscores the fact that high spatiotemporal resolution confocal live imaging provides more accurate trafficking kinetics and endosomal residence times, which might be important determinants of linker processing efficiency. In summary, METxMET Ab internalizes into sorting endosomes, rapidly reaches recycling endosomes and slowly reaches late endosomes (presumably from sorting endosomes), where it displays the longest residence time.

A protease-cleavable biosensor conjugated to METxMET Ab is primarily cleaved in late and recycling endosomes

It has been proposed that endosomes can process ADCs with protease-cleavable linkers (6, 7); however, neither the identity nor the relative contributions of the different endosomes to ADC processing have been defined. To address this question, the METxMET Ab was conjugated with a protease-cleavable biosensor (METxMET-VC-biosensor) containing one AF568 and one AF647 fluorophore tethered by a VC linker identical to that of the METxMET-VC-ADC. The intact biosensor emits only AF647 signal, because AF568 is effectively quenched via fluorescence resonance energy transfer to AF647, whereas the cleaved biosensor emits both AF568 and AF647 signals (**Fig. 2A**; ref. 27). Internalization of METxMET-VC-biosensor into EBC1 cells resulted in the appearance of red (AF647) intracellular vesicles that gradually

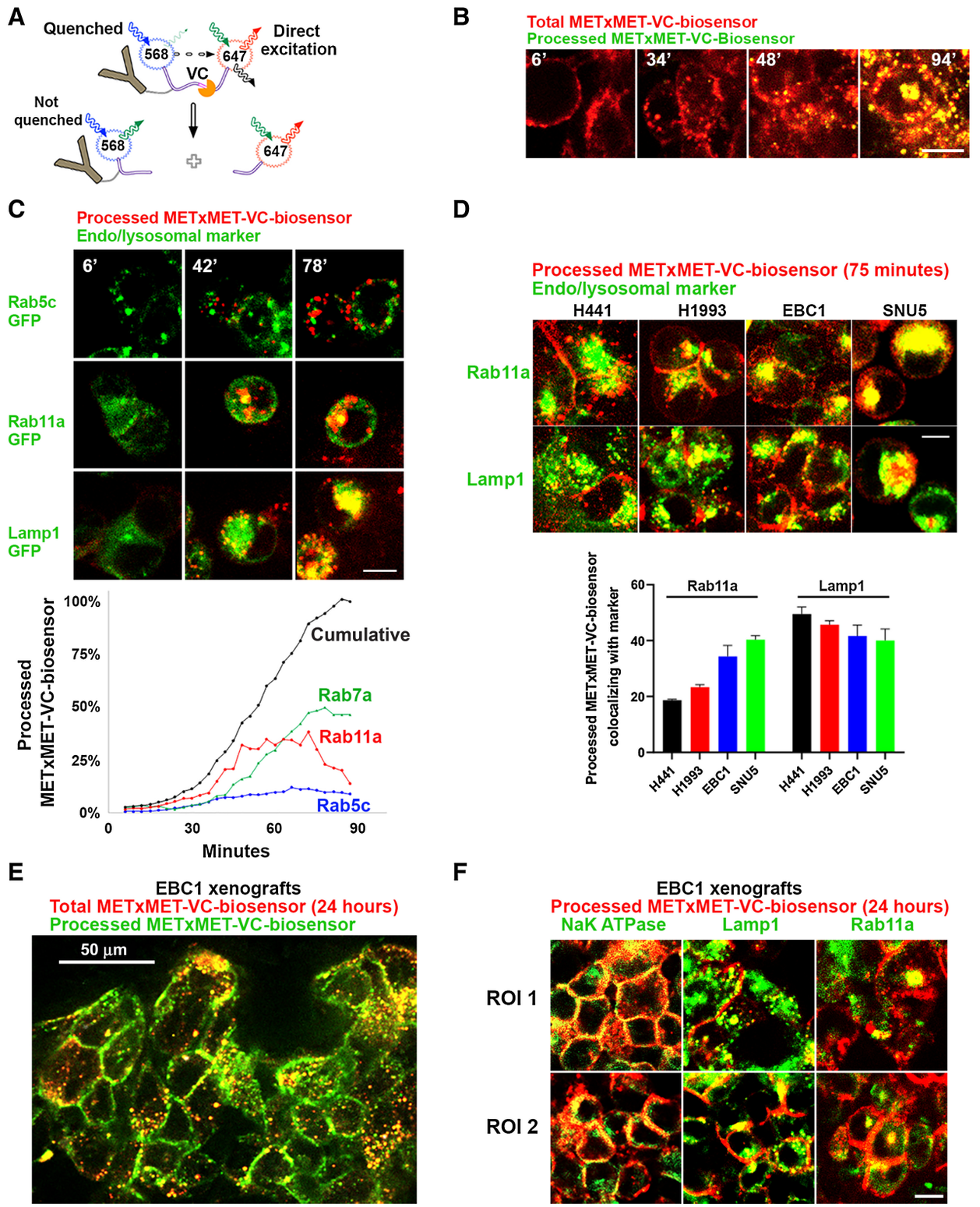

Figure 2.

METxMET-VC-biosensor traffics to and is processed in recycling and late endosomes in different cancer cells and xenografts. **A,** METxMET Ab were conjugated with a biosensor (METxMET-VC-biosensor) that contains AF568 and AF647 fluorophores tethered by a VC linker peptide identical to that of METxMET-VC-ADC. The intact biosensor emits only AF647 signal, while the processed biosensor emits both AF568 and AF647 signals (27). **B,** Internalization and processing time course of prebound METxMET-VC-biosensor in EBC1 cells. (*Continued on the following page.*)

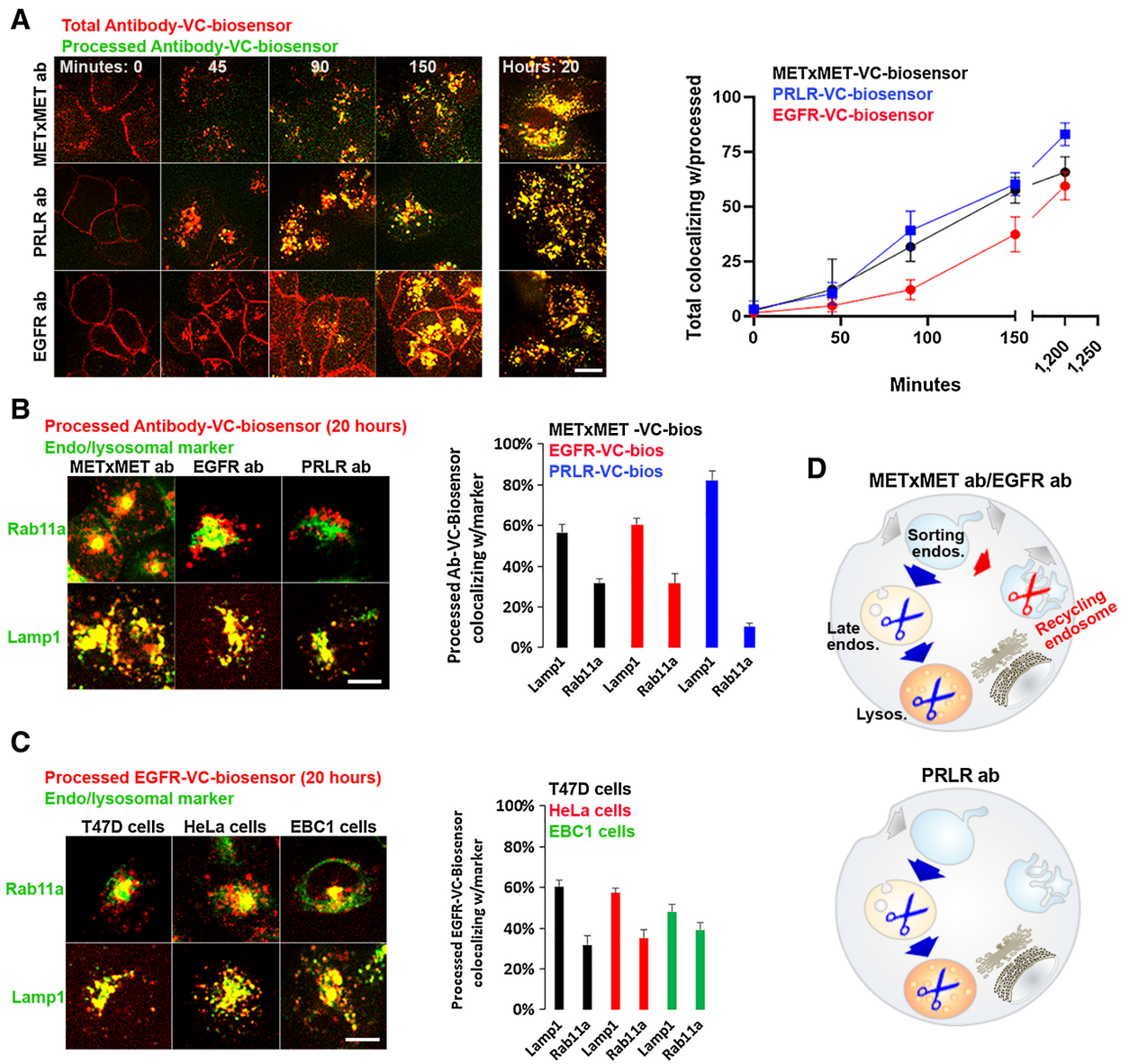

Figure 3.

Recycling endosomes can sustain VC-linker processing of different ADCs. **A,** Continuous internalization and processing time course of METxMET, PRLR, or EGFR-VC-biosensor in T47D cells. Images (left) and MCC quantification of total Ab-VC-biosensor (red) with processed Ab-VC-biosensor (green) in nine confocal fields/condition (right). **B,** A total of 20-hour continuous incubation of METxMET, EGFR, or PRLR-VC-biosensor (red) followed by immunofluorescence staining of endogenous Rab11a or Lamp1 (green) in T47D cells. Images (left) and MCC quantification in nine confocal ROIs/condition containing one to two cells (right). **C,** A total of 20-hour continuous incubation of EGFR-VC-biosensor (red) followed by immunofluorescence staining of endogenous Rab11a or Lamp1 (green) in the indicated cell lines. Images (left) and MCC quantification in nine confocal ROIs/condition containing one to two cells (right). **D,** Trafficking and processing model of METxMET, EGFR, and PRLR-VC-ADC. METxMET and EGFR traffic to and are processed in both recycling and late endosomes/lysosomes, while PRLR exclusively traffics to and is processed in late endosomes/lysosomes. Scale bar: 10 μm.

(*Continued.*) **C,** Internalization and processing time course of prebound METxMET-VC-biosensor in EBC1 cells stably expressing either Rab5c-GFP, Rab11a-GFP, or Rab7a-GFP. Processing at sorting, recycling, and late endosomes was quantified as the percentage of processed METxMET-VC-biosensor integrated fluorescence (AF568, red) colocalizing with either Rab5-GFP, Rab11-GFP, or Rab7-GFP (green). Representative images (top) and quantification (bottom) from five ROIs containing one to five cells each. **D,** A total of 75-minute continuous internalization of METxMET-VC-biosensor (red) followed by immunofluorescence staining of endogenous Rab11a or Lamp1 (green) in the indicated cell lines. Images (top) and MCC quantification in nine confocal ROIs/condition containing one to two cells (bottom). **E,** Cellular localization of total and processed METxMET-VC-biosensor in frozen sections of EBC1 xenografts 24 hours postinjection. **F,** Processed METxMET-VC-biosensor (red) colocalizing with immunofluorescence staining of endogenous NaK ATPase, Lamp1, and Rab11a (green) in EBC1 xenografts 24 hours postinjection. Two representative ROIs shown. Scale bar: 10 μm unless otherwise indicated.

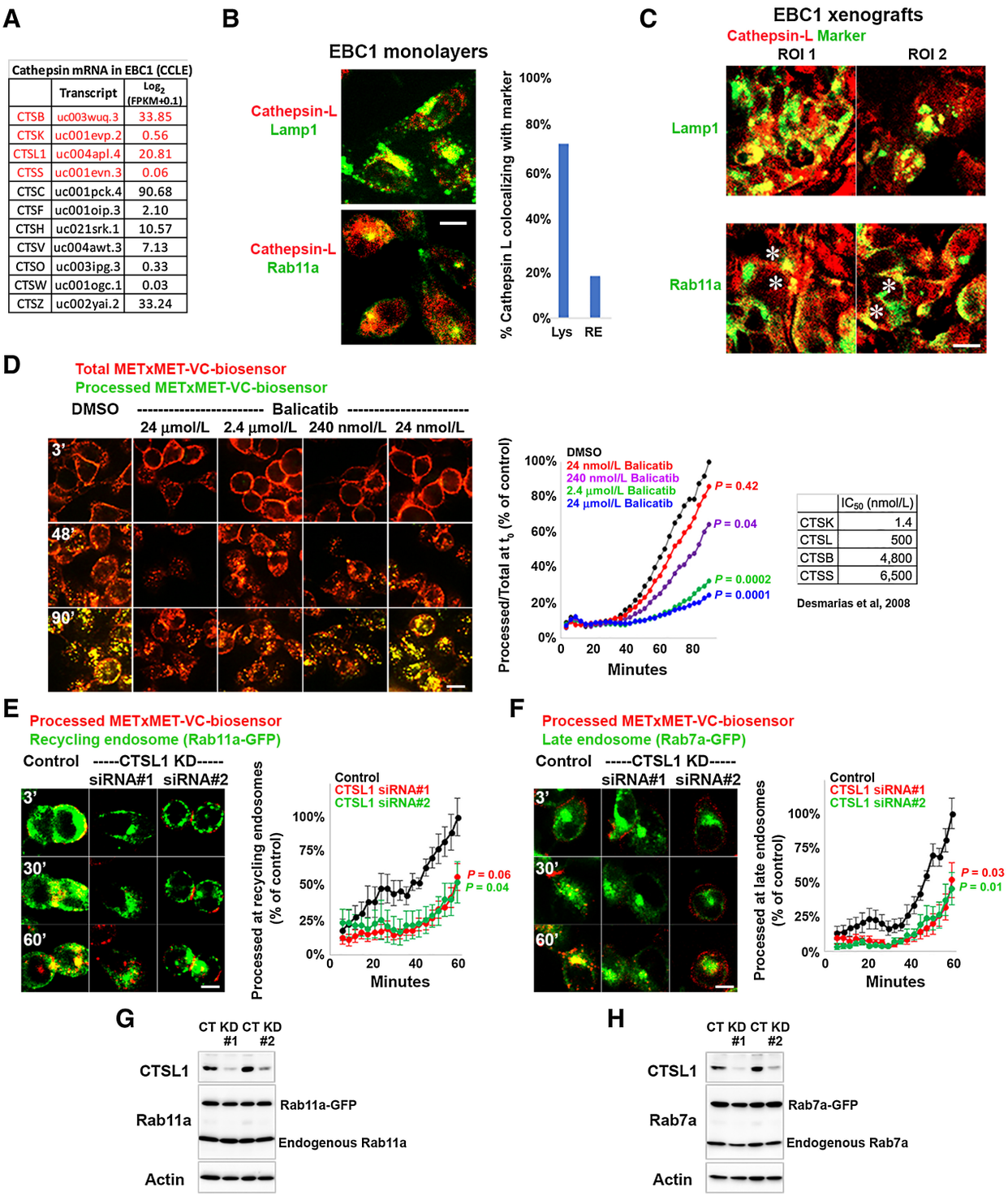

Figure 4.

A fraction of cathepsin-L1 localizes and mediates processing in recycling and late endosomes. **A,** mRNA expression of the 11 human cysteine proteases in EBC1 cells [Cancer Cell Line Encyclopedia (CCLE) database]. Proteases previously shown to process VC linkers (38) are highlighted in red. **B,** immunofluorescence staining of endogenous cathepsin-L (red) and Rab11a or Lamp1 (green) in EBC1 cells. Images (left) and MCC quantification in nine confocal fields/condition (right). **C,** Representative ROIs of immunofluorescence staining of endogenous cathepsin-L (red) and Rab11a or Lamp1 (green) in EBC1 xenografts. (*Continued on the following page.*)

turned green (AF568) upon processing of the VC linker (**Fig. 2B**). Confocal live imaging colocalization analysis showed that sorting endosomes process negligible amounts of METxMET-VC-biosensor (<10%), although this compartment is the first trafficking station for all internalized METxMET Ab. Recycling endosomes support substantial (35%) processing of METxMET-biosensor and is the only compartment in the cell where processing occurs in the first 40 minutes postinternalization. Late endosomes are the primary site of METxMET-VC-biosensor processing in the cell (50%; **Fig. 2C**). These findings indicate that processing of protease-cleavable VC linkers occurs primarily in late endosomes, with significant contribution from recycling endosomes. Sorting endosomes negligibly contribute to linker processing despite a relatively long residence time of the ADC in this compartment.

Recycling endosomes mediate METxMET ADC processing in different cancer cell types and *in vivo*

We next study whether the catalytic activity of recycling endosomes is broadly conserved in cancer cells from different lineages and *in vivo* tumor xenografts. MET-expressing NCI-H441 (lung papillary adenocarcinoma), SNU-5 (gastric carcinoma), NCI-H1993, and EBC1 (non–small cell lung cancer) cells were incubated with METxMET-VC-biosensor for 75 minutes, when processing is maximum in both recycling and late endosomes (**Fig. 2C**). Although METx-MET-VC-biosensor was primarily processed in Lamp1-positive late endosomes/lysosomes, substantial ADC processing was observed in Rab11a-positive recycling endosomes in all cell lines tested (**Fig. 2D**). The amount of ADC processing in recycling endosomes seems to be cell line dependent, possibly reflecting differences in the receptor residence time and protease concentration in this compartment across different cell types.

To determine whether recycling endosomes can sustain ADC processing *in vivo*, EBC1 xenograft-bearing mice were injected with METxMET-VC-biosensor, xenografts were harvested 24 hours after injection, and sections were processed for confocal microscopy analysis. Tumor sections scans (∼4 mm^2) showed efficient tumor penetration and processing of the METxMET-VC-biosensor in EBC1 xenografts (Supplementary Fig. S3a). Higher magnification images revealed that processed METxMET-VC-biosensor localized largely to intracellular vesicles and to the periphery of the cell (**Fig. 2E**; Supplementary Fig. S3b). The peripheral signal partially colocalized with the plasma membrane marker Na/K-ATPase (**Fig. 2F**). Processed METxMET-VC-biosensor might recycle to the cell surface after endosomal biosensor cleavage (Supplementary Fig. S3c). Long incubation times, such as the 24 hours used here, are expected to increase localization of the METxMET-VC-biosensor in the late endosomes/lysosomes. Indeed, processed METxMET-VC-biosensor localized largely to the lysosomes of EBC1 xenograft cells 24 hours after injection. However, a substantial amount of processed ADC could also be detected in recycling endosomes (**Fig. 2F**; Supplementary Fig. S3d). These results indicate that linker processing in recycling endosomes is conserved across different cancer cell types and *in vivo*.

Recycling endosomes mediate VC linker processing of EGFR, but not PRLR ADC

Our results suggest that recycling endosomes can support processing of different ADCs containing VC linker, provided that the ADC traffics to recycling endosomes. Similar to MET, the tyrosine kinase receptor EGFR recycles to the plasma membrane and there is ample evidence indicating that it traverses the recycling endosomes in a Rab11a-dependent manner (10). In contrast, PRLR is rapidly internalized and traffics directly to lysosomes, likely avoiding the recycling endosomes (11). A time course experiment was performed in T47D cells which express EGFR, PRLR, and low, yet detectable, levels of MET. After 150 minutes continuous incubation, METx-MET and PRLR-VC-biosensor underwent efficient internalization and processing. In contrast, a large fraction of the EGFR-VC-biosensor remained unprocessed at the plasma membrane. After 20 hours continuous incubation, all ADCs were almost completely internalized and processed by more than 50%, thus this time was chosen for further analysis (**Fig. 3A**). Colocalization analysis showed that METxMET and EGFR-VC-biosensor were primarily processed in Lamp1-positive late endosomes/lysosomes (56% and 60%, respectively), although substantial processing of both ADCs was observed in Rab11a-positive recycling endosomes (31% and 32%). In contrast, PRLR-VC-biosensor was almost exclusively processed by late endosomes/lysosomes (82%) with significantly less processing by recycling endosomes compared with METxMET (10%, $P < 0.0001$; **Fig. 3B**). As previously observed for METxMET, EGFR-VC-biosensor was processed by recycling endosomes in different cell lines (**Fig. 3C**), further supporting the idea that the catalytic activity of recycling endosomes is conserved across different cancer cell types. These data suggest that recycling endosomes might play an important role in enhancing the processing of multiple ADCs (**Fig. 3D**).

Cathepsin-L is partially responsible for METxMET ADC processing in recycling and late endosomes

To shed light on the mechanism underlying the catalytic activity of recycling endosomes, we compared the role of cysteine proteases in VC linker processing specifically in recycling and late endosomes. Six of the 11 human cysteine proteases (cathepsin B, C, H, V, Z, and L) are expressed in EBC1 cells (**Fig. 4A**) but only two of them (B and L) have been shown to process VC linkers (8). Cathepsin-L (CTSL1) displayed a strong immunofluorescence signal in EBC1 cells that largely localized to late endosomes/lysosomes, although up to 20% could be detected in recycling endosomes *in vitro* and *in vivo* (**Fig. 4B** and **C**, asterisks). A small-molecule inhibitor of cathepsins K, B, S, and L partially delayed METxMET-VC-biosensor processing at a concentration compatible with

(*Continued.*) **D,** Internalization and processing time course of prebound METxMET-VC-biosensor in balicatib-treated EBC1 cells. Processed METxMET-VC-biosensor was quantified by the MFI of AF568 (green) over that of AF647 (red) at t0 and normalized to control. Representative images (left) and quantification (right) from nine confocal fields/condition. Internalization and processing time course of prebound METxMET-VC-biosensor in control and cathepsin-L siRNA knockdown EBC1cells stably expressing Rab11a-GFP (**E**) or Rab7a-GFP (**F**). Processing at recycling or late endosomes was quantified as the percentage of processed METxMET-VC-biosensor integrated fluorescence (AF568, red) colocalizing with either Rab11-GFP or Rab7-GFP (green). Representative images (left) and quantification (right) from five ROIs/condition containing one to five cells each. WB analysis showing transient cathepsin-L1 siRNA knockdown in EBC1cells stably expressing Rab11a-GFP (**G**) or Rab7a-GFP (**H**). Scale bar: 10 μm. *t* test versus control.

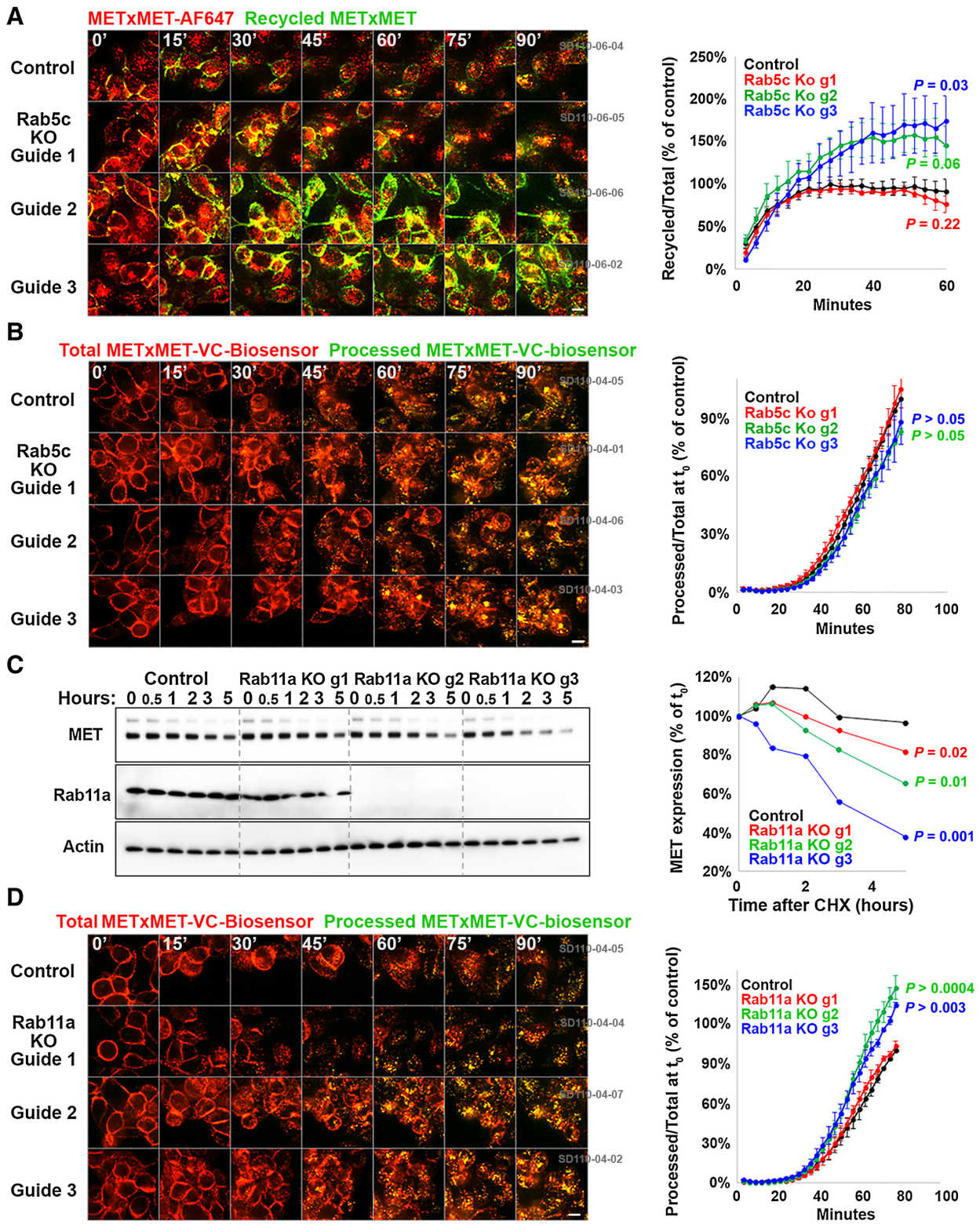
A
METxMET-AF647 Recycled METxMET
0' 15' 30' 45' 60' 75' 90'
Control
Rab5c KO Guide 1
Guide 2
Guide 3
SD110-06-04
SD110-06-05
SD110-06-06
SD110-06-02
Recycled/Total (% of control)
250%
200%
150%
100%
50%
0%
0 20 40 60
Minutes
Control
Rab5c Ko g1
Rab5c Ko g2
Rab5c Ko g3
P = 0.03
P = 0.06
P = 0.22
B
Total METxMET-VC-Biosensor Processed METxMET-VC-biosensor
0' 15' 30' 45' 60' 75' 90'
Control
Rab5c KO Guide 1
Guide 2
Guide 3
SD110-04-05
SD110-04-01
SD110-04-06
SD110-04-03
Processed/Total at t0 (% of control)
90%
60%
30%
0%
0 20 40 60 80 100
Minutes
Control
Rab5c Ko g1
Rab5c Ko g2
Rab5c Ko g3
P > 0.05
P > 0.05
C
Control Rab11a KO g1 Rab11a KO g2 Rab11a KO g3
Hours: 0 0.5 1 2 3 5 0 0.5 1 2 3 5 0 0.5 1 2 3 5 0 0.5 1 2 3 5
MET
Rab11a
Actin
MET expression (% of t0)
120%
100%
80%
60%
40%
20%
0 2 4
Time after CHX (hours)
Control
Rab11a KO g1
Rab11a KO g2
Rab11a KO g3
P = 0.02
P = 0.01
P = 0.001
D
Total METxMET-VC-Biosensor Processed METxMET-VC-biosensor
0' 15' 30' 45' 60' 75' 90'
Control
Rab11a KO Guide 1
Guide 2
Guide 3
SD110-04-05
SD110-04-04
SD110-04-07
SD110-04-02
Processed/Total at t0 (% of control)
150%
100%
90%
60%
30%
0%
0 20 40 60 80 100
Minutes
Control
Rab11a KO g1
Rab11a KO g2
Rab11a KO g3
P > 0.0004
P > 0.003

cathepsin-L inhibition (**Fig. 4D**; ref. 38). To determine whether cathepsin-L mediates processing in recycling endosomes, cathepsin-L expression was knocked down in EBC1 cells stably expressing either Rab11a-GFP or Rab7a-GFP (**Fig. 4G** and **H**) and METxMET-VC-biosensor processing was quantified with confocal live imaging. At the whole cell level, cathepsin-L knockdown delayed METxMET-VC-biosensor processing in the two engineered cell lines (Supplementary Fig. S4a and S4b). Importantly, cathepsin-L knockdown delayed METxMET-VC-biosensor processing in recycling endosomes with comparable efficiency to late endosomes (**Fig. 4E** and **F**). Taken together, these results suggest that up to 20% of cathepsin-L is "missorted" to the recycling endosomes, where it processes VC linkers, but it is not sufficient to completely degrade the antibody, which returns to the plasma membrane as measured in our recycling assays (**Fig. 5A**). These findings shed light on the mechanism underlying a therapeutically relevant catalytic activity of recycling endosomes and provides a direct observation of the catalytic effect of a cysteine protease in this compartment.

The Rab5c and Rab11a GTPases regulate transendosomal trafficking and processing of METxMET ADC

To establish a direct link between ADC trafficking and processing, we studied the functional effect of CRISPR-mediated Rab5c or Rab11a deletion on METxMET-VC-biosensor processing. In agreement with previous reports (31, 33), METxMET Ab internalization was not affected by either Rab5c or Rab11a deletion (Supplementary Fig. S5a). Rab5c deletion (Supplementary Fig. S5b) increased METxMET Ab recycling (**Fig. 5A**), thus explaining the higher cell surface levels of METxMET observed in our CRISPR screen. The increase in recycling was evident between 20 and 40 minutes, a time compatible with the slow recycling pathway that traverses recycling endosomes. Redirecting METxMET-VC-biosensor trafficking to the recycling endosomes (through Rab5c deletion) caused only a negligible reduction in biosensor processing (**Fig. 5B**), providing further support for the catalytic activity of recycling endosomes. These results also suggest that METxMET-VC-biosensor is efficiently processed before being recycled back to the plasma membrane.

In contrast to Rab5c, Rab11a deletion increased the rate of MET degradation (**Fig. 5C**), consistent with the lower levels of cell surface METxMET Ab observed in our screen. Rab11a deletion also increased METxMET-VC-biosensor processing, suggesting increased trafficking to late endosomes (**Fig. 5D**). Rab11a might have a broader role on tyrosine kinase receptor trafficking, since its deletion also increased EGFR degradation, a known Rab11a cargo (39, 40), but had a small effect on HER2 degradation (Supplementary Fig. S5c).

These data further support the contention that late and recycling endosomes are the two primary sites of processing for protease-cleavable linkers.

Transendosomal trafficking is required for METxMET ADC processing and cytotoxicity

To dissect the effect of transendosomal trafficking on METxMET-VC-ADC processing and killing efficacy, we set out to identify compounds that potently disrupt transendosomal trafficking with little effect on internalization. Using a small-molecule library containing inhibitors of intracellular trafficking processes and a novel triple colocalization analysis, we did not detect any effect on METxMET-VC-biosensor internalization or processing after inhibition of the secretory pathway (monensin, brefeldin A), cholesterol raft formation (simvastatin), PI3K function (LY294002), proteosomal degradation (bortezomib, lactasistin), microtubule organization (nocodazole), or actin polymerization (CK666, CK869) or depolymerization (phalloidin, narciclasine; Supplementary Fig. S6a). As expected, inhibiting internalization (chaetoglobisin A) or endosomal/lysosomal acidification (bafilomycin A and chloroquine) reduced METxMET-VC-biosensor processing. Interestingly, dynasore potently inhibited METxMET-VC-biosensor processing but appeared to have only a negligible effect on internalization (Supplementary Fig. S6a). Dynasore caused only a slight and transient inhibition of METxMET Ab internalization, but appeared to promote a redistribution of internalized METxMET Ab from perinuclear to peripheral after 45–75 minutes (**Fig. 6A**), suggesting a specific effect on transendosomal trafficking (41). Indeed, dynasore potently delayed METxMET-VC-biosensor exit from sorting endosomes and arrival to recycling and late endosomes (**Fig. 6B**; Supplementary Fig. S6b). Failure to reach recycling and late endosomes completely blocked biosensor processing (**Fig. 6C**; Supplementary Fig. S6c) and inhibited METxMET-VC-ADC-induced apoptosis (**Fig. 6D**). The potency of apoptosis inhibition induced by dynasore was similar to that of bafilomycin A and chaetoglobosin A, suggesting that transendosomal trafficking is as important as internalization and endosomal/lysosomal acidification for ADC efficacy (Supplementary Fig. S6d). These data indicate that recycling and late endosomes play an essential role in ADC processing and the induction of cytotoxicity (**Fig. 6E**).

Discussion

Although ADCs with protease-cleavable linkers constitute a majority of the ADCs currently in clinical development (5), it remains unclear whether these cleavable linker/payloads can be efficiently processed in endosomes. In addition, it is not known which of the many endosomal compartments of cells can perform this task and what their relative contribution to processing is. In this study, we show that a clinical-stage METxMET Ab is internalized into sorting endosomes, rapidly transported to recycling endosomes and slowly transported to late endosomes. Although late endosomes are the primary site of processing of ADCs containing a VC linker biosensor, 35% of linker processing occurs in recycling endosomes, partly mediated by

Figure 5.
The Rab5c and Rab11a GTPases regulate transendosomal trafficking and linker processing of METxMET-VC-biosensor. **A,** Prebound METxMET-AF647 was allowed to internalize for 60 minutes in control and Rab5c knockout (KO) EBC1/Cas9 cells. Recycling of internalized METxMET-AF647 (red) was determined by continuous incubation with anti-human-AF488 Fab (green) during confocal live imaging acquisition. METxMET-AF647 recycling was quantified as the recycled to total METxMET Ab ratio normalized to control. Representative images (left) and quantification (right) from nine confocal fields/condition. Internalization and processing time course of prebound METxMET-VC-biosensor in control and Rab5c KO (**B**) or Rab11a KO (**D**) EBC1/Cas9 cells. Processed METxMET-VC-biosensor was quantified by the MFI of AF568 (green) over that of AF647 (red) at t0 and normalized to control. Representative images (left) and quantification (right) from nine confocal fields/condition. **C,** Cycloheximide chase assay showing that Rab11a KO promotes c-Met degradation in EBC1/Cas9 cells. Blot (left) and quantification (right). Scale bar: 10 μm. *t* test versus control.

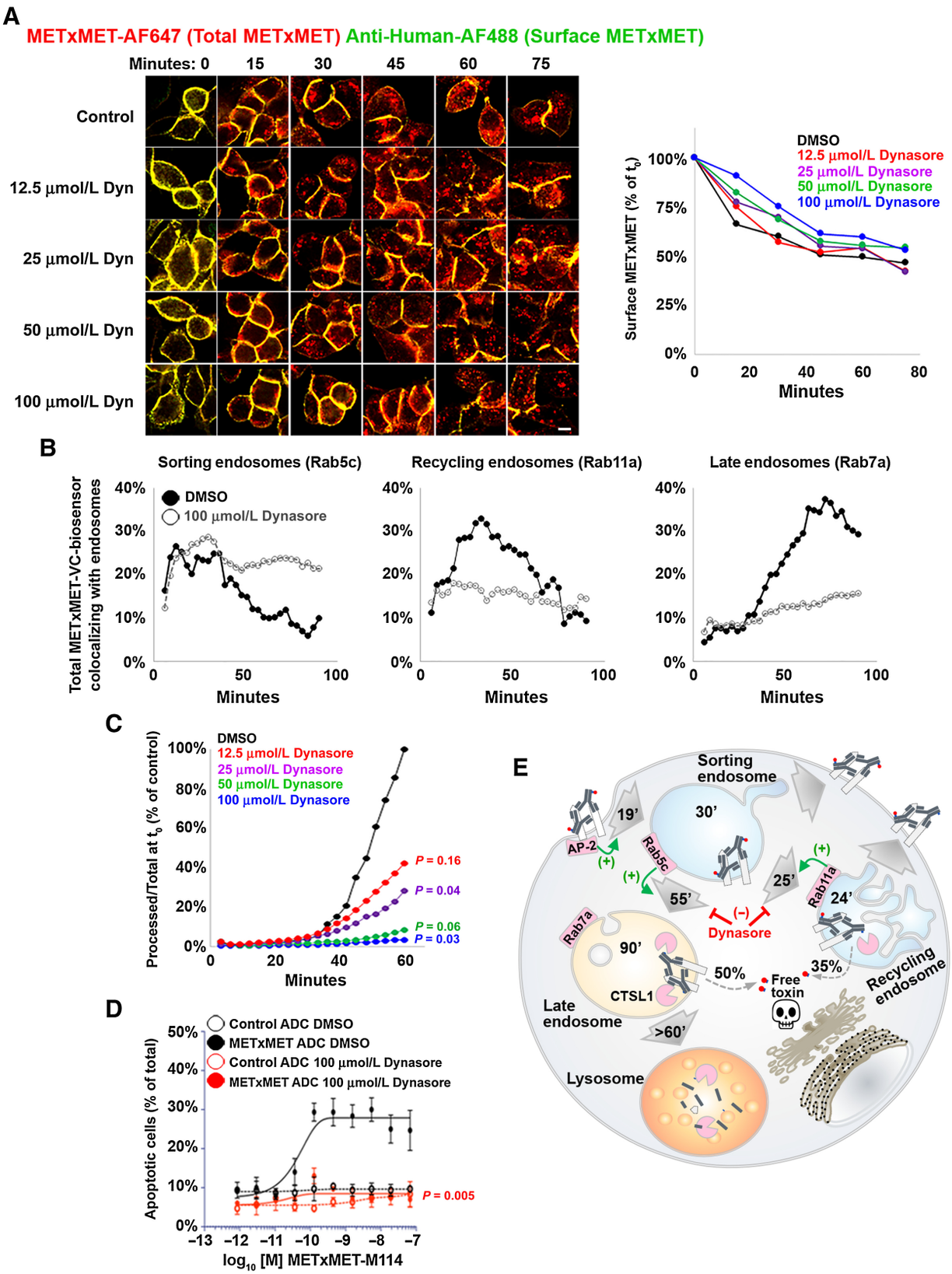
A
METxMET-AF647 (Total METxMET) Anti-Human-AF488 (Surface METxMET)
Minutes: 0 15 30 45 60 75
Control
12.5 μmol/L Dyn
25 μmol/L Dyn
50 μmol/L Dyn
100 μmol/L Dyn
Surface METxMET (% of t0)
DMSO
12.5 μmol/L Dynasore
25 μmol/L Dynasore
50 μmol/L Dynasore
100 μmol/L Dynasore
Minutes
B
Sorting endosomes (Rab5c)
Recycling endosomes (Rab11a)
Late endosomes (Rab7a)
Total METxMET-VC-biosensor colocalizing with endosomes
DMSO
100 μmol/L Dynasore
Minutes
C
Processed/Total at t0 (% of control)
DMSO
12.5 μmol/L Dynasore
25 μmol/L Dynasore
50 μmol/L Dynasore
100 μmol/L Dynasore
P = 0.16
P = 0.04
P = 0.06
P = 0.03
Minutes
D
Apoptotic cells (% of total)
Control ADC DMSO
METxMET ADC DMSO
Control ADC 100 μmol/L Dynasore
METxMET ADC 100 μmol/L Dynasore
P = 0.005
log10 [M] METxMET-M114
E
Sorting endosome
19'
30'
AP-2
Rab5c
(+)
55'
25'
Rab11a
24'
(-)
Dynasore
Rab7a
90'
50%
35%
Free toxin
CTSL1
Late endosome
>60'
Recycling endosome
Lysosome

cathepsin-L. Blocking METxMET ADC trafficking from sorting to recycling and late endosomes inhibits linker processing and ADC-mediated cytotoxicity, underscoring the importance of transendosomal trafficking for ADC efficacy. Our findings suggest that receptors that recycle through recycling endosomes might be suitable targets for cleavable ADCs.

Mechanistically, our data indicate that METxMET is internalized into sorting endosomes by the clathrin adaptor AP-2 (30), transported to late endosomes by Rab5c (31, 34) and to recycling endosomes by Rab11a (33, 42) and its effector Rab11-FIP5 (43, 44). Tsui and colleagues had proposed sorting endosomes as a potential site of linker processing rapidly after internalization (7). Similarly, we found that METxMET-VC linker processing starts rapidly after internalization. Using spatiotemporal analysis with confocal live imaging our study revealed that although the cleavable METxMET Ab reaches both sorting and recycling endosomes at similar times, most of the early processing occurs in recycling endosomes. Furthermore, processing in recycling endosomes seems to be widely conserved among different cancer cell types and targets, but it is specific to recycling receptors (METxMET and EGFR; refs. 10, 21) and does not contribute to the processing of ADCs targeted to the lysosomes (PRLR; ref. 11). The identification of functionally active cathepsin-L in recycling endosomes further supports the notion of VC linker processing in this compartment. Although the mechanism by which cathepsin-L reaches recycling endosomes remains unclear, overexpression of cysteine proteases in cancer might saturate the normal trans-Golgi to late endosome pathway (45), resulting in *"missorting"* to recycling endosomes. Given that sorting endosomes promote recycling endosome biogenesis (46, 47) and perform recycling (12), the discovery of the catalytic function of recycling endosomes provides an ontological explanation for the evolution of this compartment.

On a translational level, our study provides information for the rational design of ADCs: it suggests that cleavable linker payloads are suitable not only for ADCs that traffic toward the degradative pathway, but also for ADCs that traverse recycling endosomes with a recycling rate slower than the processing rate. Specifically, our kinetic data suggest that ADCs need to remain at the recycling endosomes for 10–15 minutes to be efficiently processed. After processing in the recycling endosomes, permeable payloads might translocate to the cytosol directly while impermeable payloads might require specific transporters localized in this compartment. Upon recycling to the plasma membrane, processed ADCs with pH-dependent binding might be released from the target, thus allowing the target to bind and deliver another intact ADC molecule (12, 48). An example with ample clinical evidence supporting the use of cleavable linkers with recycling receptors is that of the two HER2-ADCs: the noncleavable trastuzumab-MCC-DM1 and the cleavable trastuzumab-GGFG-DxD. In a recent side-by-side comparison in patients with breast cancer, the latter was more efficacious than the first (49). Given that trastuzumab fast recycling limits the efficacy of trastuzumab-MCC-DM1 (1), it is tempting to speculate that endosomal linker processing might partially explain the better efficacy of trastuzumab-GGFG-DxD. On the other hand, cleavable linkers might not confer additional benefits to ADCs that are targeted to lysosomes, as suggested by a PRLR ADC containing a noncleavable linker that showed potent anti-tumor efficacy in preclinical models (50).

Our findings uncover a novel catalytic activity of recycling endosomes, provide insight into the relationship between transendosomal trafficking and ADC processing and suggest that recycling receptors can efficiently deliver ADC payloads into tumor cells. These results may potentially broaden the spectrum of available ADC targets for cancer therapy.

Authors' Disclosures

A.E. Perez Bay reports other support from Regeneron Pharmaceuticals during the conduct of the study; in addition, A.E. Perez Bay has a patent for US20210246224A1 pending to Regeneron Pharmaceuticals Inc and a patent for AU2021228225A1 pending to Regeneron Pharmaceuticals Inc. D. Faulkner reports personal fees from Regeneron Pharmaceuticals Inc. during the conduct of the study. J.O. DaSilva reports a patent for MET antibodies pending to Regeneron Pharmaceuticals pending; and is an employee of Regeneron Pharmaceuticals. J.T. Giurleo reports personal fees from Regeneron Pharmaceuticals during the conduct of the study. G. Thurston is an employee and shareholder of Regeneron Pharmaceuticals. C. Daly reports a patent for MET antibodies pending to Regeneron Pharmaceuticals, Inc. No disclosures were reported by the other authors.

Authors' Contributions

A.E. Perez Bay: Conceptualization, resources, data curation, formal analysis, supervision, investigation, methodology, writing–original draft, writing–review and editing. **D. Faulkner:** Data generation. **J.O. DaSilva:** Resources. **T.M. Young:** Resources. **K. Yang:** Resources. **J.T. Giurleo:** Resources. **D. Ma:** Resources. **F.J. Delfino:** Resources. **W.C. Olson:** Resources. **G. Thurston:** Supervision, writing–review and editing. **C. Daly:** Conceptualization, supervision, writing–review and editing. **J. Andreev:** Supervision, writing–review and editing.

Acknowledgments

This work has been funded by Regeneron Pharmaceuticals.

The publication costs of this article were defrayed in part by the payment of publication fees. Therefore, and solely to indicate this fact, this article is hereby marked "advertisement" in accordance with 18 USC section 1734.

Note

Supplementary data for this article are available at Molecular Cancer Therapeutics Online (http://mct.aacrjournals.org/).

Received June 16, 2022; revised October 18, 2022; accepted January 6, 2023; published first January 11, 2023.

Figure 6.

Transendosomal trafficking promotes METxMET ADC processing and killing efficacy. **A,** Prebound METxMET-AF647 (red) allowed to internalize in dynasore-treated EBC1 cells and subsequently stained with anti-human-AF488 Fab (surface METxMET, green). Surface METxMET was quantified by the colocalization of METxMET-AF647 with anti-human-AF488 Fab using MCC and normalized to t0. Representative images (left) and quantification (right) from nine confocal fields/condition. **B,** Internalization time course of prebound METxMET-VC-biosensor in dynasore-treated EBC1 cells stably expressing either Rab5c-GFP, Rab11a-GFP, or Rab7a-GFP. Trafficking to sorting, recycling, or late endosomes was quantified by the MCC quantification of total METxMET-VC-biosensor (AF647) with Rab5c-GFP, Rab11a-GFP, or Rab7a-GFP, respectively, in five ROIs/condition containing one to five cells each. Images provided in Supplementary Fig. S6b. **C,** Processing time course of prebound METxMET-VC-biosensor in dynasore-treated EBC1 cells. Processed METxMET-VC-biosensor was quantified by the MFI of AF568 (green) over that of AF647 (red) at t0 and normalized to control in nine confocal fields/condition. Images provided in Supplementary Fig. S6c. **D,** EBC1/Cas9 cells were treated for 24 hours with the indicated concentrations of METxMET-VC-ADC or Control-VC-ADC and a caspase 3/7 dye. Percentage of apoptotic cells was determined as the ratio of caspase 3/7-positive cells over Hoechst-positive cells using high-content microscopy and a segmentation algorithm. **E,** Trafficking model showing the molecular machinery, endosomal itinerary, residence time, and relative cleavage of METxMET ADC in sorting, recycling, and late endosomes. Scale bar: 10 μm. *t* test versus control.

References

1. Austin CD, De Mazière AM, Pisacane PI, van Dijk SM, Eigenbrot C, Sliwkowski MX, et al. Endocytosis and sorting of ErbB2 and the site of action of cancer therapeutics trastuzumab and geldanamycin. Mol Biol Cell 2004;15:5268–82.
2. Chalouni C, Doll S. Fate of antibody-drug conjugates in cancer cells. J Exp Clin Cancer Res 2018;37:20.
3. Ritchie M, Tchistiakova L, Scott N. Implications of receptor-mediated endocytosis and intracellular trafficking dynamics in the development of antibody drug conjugates. MAbs 2013;5:13–21.
4. Lonial S, Lee HC, Badros A, Trudel S, Nooka AK, Chari A, et al. Longer term outcomes with single-agent belantamab mafodotin in patients with relapsed or refractory multiple myeloma: 13-month follow-up from the pivotal DREAMM-2 study. Cancer 2021;127:4198–212.
5. Lyon R. Drawing lessons from the clinical development of antibody-drug conjugates. Drug Discov Today Technol 2018;30:105–9.
6. Mohamed MM, Sloane BF. Cysteine cathepsins: multifunctional enzymes in cancer. Nat Rev Cancer 2006;6:764–75.
7. Tsui CK, Barfield RM, Fischer CR, Morgens DW, Li A, Smith BAH, et al. CRISPR-Cas9 screens identify regulators of antibody-drug conjugate toxicity. Nat Chem Biol 2019;15:949–58.
8. Caculitan NG, dela Cruz Chuh J, Ma Y, Zhang D, Kozak KR, Liu Y, et al. Cathepsin B is dispensable for cellular processing of cathepsin B-cleavable antibody-drug conjugates. Cancer Res 2017;77:7027–37.
9. Graziani EI, Sung M, Ma D, Narayanan B, Marquette K, Puthenveetil S, et al. PF-06804103, a site-specific anti-HER2 antibody-drug conjugate for the treatment of HER2-expressing breast, gastric, and lung cancers. Mol Cancer Ther 2020;19:2068–78.
10. Sorkin A, Goh LK. Endocytosis and intracellular trafficking of ErbBs. Exp Cell Res 2008;314:3093–106.
11. Andreev J, Thambi N, Perez Bay AE, Delfino F, Martin J, Kelly MP, et al. Bispecific antibodies and antibody-drug conjugates (ADCs) bridging HER2 and prolactin receptor improve efficacy of HER2 ADCs. Mol Cancer Ther 2017;16:681–93.
12. Maxfield FR, McGraw TE. Endocytic recycling. Nat Rev Mol Cell Biol 2004;5:121–32.
13. Barlowe C, Schekman R. SEC12 encodes a guanine-nucleotide-exchange factor essential for transport vesicle budding from the ER. Nature 1993;365:347–9.
14. Kreitzer G, Myat MM. Microtubule motors in establishment of epithelial cell Polarity. Cold Spring Harb Perspect Biol 2018;10:a027896.
15. McNally KE, Cullen PJ. Endosomal retrieval of cargo: retromer is not alone. Trends Cell Biol 2018;28:807–22.
16. Stenmark H. Rab GTPases as coordinators of vesicle traffic. Nat Rev Mol Cell Biol 2009;10:513–25.
17. Traub LM, Bonifacino JS. Cargo recognition in clathrin-mediated endocytosis. Cold Spring Harb Perspect Biol 2013;5:a016790.
18. Wandinger-Ness A, Zerial M. Rab proteins and the compartmentalization of the endosomal system. Cold Spring Harb Perspect Biol 2014;6:a022616.
19. Weisz OA, Rodriguez-Boulan E. Apical trafficking in epithelial cells: signals, clusters and motors. J Cell Sci 2009;122:4253–66.
20. DaSilva JO, Yang K, Surriga O, Nittoli T, Kunz A, Franklin MC, et al. A biparatopic antibody-drug conjugate to treat MET-expressing cancers, including those that are unresponsive to MET pathway blockade. Mol Cancer Ther 2021;20:1966–76.
21. DaSilva JO, Yang K, Perez Bay AE, Andreev J, Ngoi P, Pyles E, et al. A biparatopic antibody that modulates MET trafficking exhibits enhanced efficacy compared with parental antibodies in MET-driven tumor models. Clin Cancer Res 2020;26:1408–19.
22. Murphy AJ, Macdonald LE, Stevens S, Karow M, Dore AT, Pobursky K, et al. Mice with megabase humanization of their immunoglobulin genes generate antibodies as efficiently as normal mice. Proc Natl Acad Sci U S A 2014;111:5153–8.
23. Zhang L, Castanaro C, Luan B, Yang K, Fan L, Fairhurst JL, et al. ERBB3/HER2 signaling promotes resistance to EGFR blockade in head and neck and colorectal cancer models. Mol Cancer Ther 2014;13:1345–55.
24. Smith EJ, Olson K, Haber LJ, Varghese B, Duramad P, Tustian AD, et al. A novel, native-format bispecific antibody triggering T-cell killing of B-cells is robustly active in mouse tumor models and cynomolgus monkeys. Sci Rep 2015;5:17943.
25. Hamblett KJ, Senter PD, Chace DF, Sun MMC, Lenox J, Cerveny CG, et al. Effects of drug loading on the antitumor activity of a monoclonal antibody drug conjugate. Clin Cancer Res 2004;10:7063–70.
26. Perez Bay AE, Schreiner R, Benedicto I, Paz Marzolo M, Banfelder J, Weinstein AM, et al. The fast-recycling receptor Megalin defines the apical recycling pathway of epithelial cells. Nat Commun 2016;7:11550.
27. Haber L, Olson K, Kelly MP, Crawford A, DiLillo DJ, Tavaré R, et al. Generation of T-cell-redirecting bispecific antibodies with differentiated profiles of cytokine release and biodistribution by CD3 affinity tuning. Sci Rep 2021;11:14397.
28. Perez Bay AE, Schreiner R, Benedicto I, Rodriguez-Boulan EJ. Galectin-4-mediated transcytosis of transferrin receptor. J Cell Sci 2014;127:4457–69.
29. Perez Bay AE, Schreiner R, Mazzoni F, Carvajal-Gonzalez JM, Gravotta D, Perret E, et al. The kinesin KIF16B mediates apical transcytosis of transferrin receptor in AP-1B-deficient epithelia. EMBO J 2013;32:2125–39.
30. Su Z, Han Y, Sun Q, Wang X, Xu T, Xie W, et al. Anti-MET VHH pool overcomes MET-targeted cancer therapeutic resistance. Mol Cancer Ther 2019;18:100–11.
31. Barbera S, Nardi F, Elia I, Realini G, Lugano R, Santucci A, et al. The small GTPase Rab5c is a key regulator of trafficking of the CD93/Multimerin-2/beta1 integrin complex in endothelial cell adhesion and migration. Cell Commun Signal 2019;17:55.
32. Goldenring JR. Recycling endosomes. Curr Opin Cell Biol 2015;35:117–22.
33. Ren M, Xu G, Zeng J, De Lemos-Chiarandini C, Adesnik M, Sabatini DD. Hydrolysis of GTP on rab11 is required for the direct delivery of transferrin from the pericentriolar recycling compartment to the cell surface but not from sorting endosomes. Proc Natl Acad Sci U S A 1998;95:6187–92.
34. Wang L, Li C, Zhang X, Yang M, Wei S, Huang Y, et al. The small GTPase Rab5c exerts bi-function in Singapore grouper iridovirus infections and cellular responses in the grouper, Epinephelus coioides. Front Immunol 2020;11:2133.
35. Barbero P, Bittova L Pfeffer SR. Visualization of Rab9-mediated vesicle transport from endosomes to the trans-Golgi in living cells. J Cell Biol 2002;156:511–8.
36. Rink J, Ghigo E, Kalaidzidis Y, Zerial M. Rab conversion as a mechanism of progression from early to late endosomes. Cell 2005;122:735–49.
37. Sönnichsen B, De Renzis S, Nielsen E, Rietdorf J, Zerial M. Distinct membrane domains on endosomes in the recycling pathway visualized by multicolor imaging of Rab4, Rab5, and Rab11. J Cell Biol 2000;149:901–14.
38. Desmarais S, Black WC, Oballa R, Lamontagne S, Riendeau D, Tawa P, et al. Effect of cathepsin k inhibitor basicity on in vivo off-target activities. Mol Pharmacol 2008;73:147–56.
39. Baumdick M, Brüggemann Y, Schmick M, Xouri G, Sabet O, Davis L, et al. EGF-dependent re-routing of vesicular recycling switches spontaneous phosphorylation suppression to EGFR signaling. Elife 2015;4:e12223.
40. Fraser J, Simpson J, Fontana R, Kishi-Itakura C, Ktistakis NT, Gammoh N. Targeting of early endosomes by autophagy facilitates EGFR recycling and signalling. EMBO Rep 2019;20:e47734.
41. Mesaki K, Tanabe K, Obayashi M, Oe N, Takei K. Fission of tubular endosomes triggers endosomal acidification and movement. PLoS One 2011;6:e19764.
42. Lapierre LA, Goldenring JR. Interactions of myosin vb with Rab11 family members and cargoes traversing the plasma membrane recycling system. Methods Enzymol 2005;403:715–23.
43. Naslavsky N, Rahajeng J, Sharma M, Jović M, Caplan S. Interactions between EHD proteins and Rab11-FIP2: a role for EHD3 in early endosomal transport. Mol Biol Cell 2006;17:163–77.
44. Schafer JC, McRae RE, Manning EH, Lapierre LA, Goldenring JR. Rab11-FIP1A regulates early trafficking into the recycling endosomes. Exp Cell Res 2016;340:259–73.
45. Hille-Rehfeld A. Mannose 6-phosphate receptors in sorting and transport of lysosomal enzymes. Biochim Biophys Acta 1995;1241:177–94.
46. Delevoye C, Miserey-Lenkei S, Montagnac G, Gilles-Marsens F, Paul-Gilloteaux P, Giordano F, et al. Recycling endosome tubule morphogenesis from sorting endosomes requires the kinesin motor KIF13A. Cell Rep 2014;6:445–54.
47. Zeigerer A, Gilleron J, Bogorad RL, Marsico G, Nonaka H, Seifert S, et al. Rab5 is necessary for the biogenesis of the endolysosomal system in vivo. Nature 2012;485:465–70.
48. Ahn G, Banik SM, Miller CL, Riley NM, Cochran JR, Bertozzi CR. LYTACs that engage the asialoglycoprotein receptor for targeted protein degradation. Nat Chem Biol 2021;17:937–46.
49. Cortés J, Kim S-B, Chung W-P, Im S-A, Park YH, Hegg R, et al. Trastuzumab deruxtecan versus trastuzumab emtansine for breast cancer. N Engl J Med 2022;386:1143–54.
50. Kelly MP, Hickey C, Makonnen S, Coetzee S, Jalal S, Wang Y, et al. Preclinical activity of the novel anti-prolactin receptor (PRLR) antibody-drug conjugate REGN2878-DM1 in PRLR-positive breast cancers. Mol Cancer Ther 2017;16:1299–311.